

PAPER

Multi-messenger observations of thunderstorm-related bursts of cosmic rays

To cite this article: A. Chilingarian *et al* 2022 *JINST* **17** P07022

View the [article online](#) for updates and enhancements.

You may also like

- [Simulations of the secondary cosmic ray propagation in the thunderstorm atmospheres resulting in the Thunderstorm ground enhancements \(TGEs\)](#)
Ashot Chilingarian and Levon Vanyan
- [Lower positive charge region \(LPCR\) and its influence on initiation of Thunderstorm ground enhancements \(TGEs\) and cloud-to-ground \(CG-\) and intracloud \(IC-\) lightning occurrences](#)
Ashot Chilingarian and Hripsime Mkrtchyan
- [Lightning origination and thunderstorm ground enhancements terminated by the lightning flash](#)
A. Chilingarian, G. Hovsepyan, G. Khanikyan *et al*.



ECS Membership = Connection

ECS membership connects you to the electrochemical community:

- Facilitate your research and discovery through ECS meetings which convene scientists from around the world;
- Access professional support through your lifetime career;
- Open up mentorship opportunities across the stages of your career;
- Build relationships that nurture partnership, teamwork—and success!

Join ECS!

Visit electrochem.org/join



Multi-messenger observations of thunderstorm-related bursts of cosmic rays

**A. Chilingarian,* G. Hovsepyan, T. Karapetyan, Y. Khanykyanc, D. Pokhsraryan,
B. Sargsyan, S. Chilingaryan and S. Soghomonyan**

*A. Alikhanyan National Lab (Yerevan Physics Institute),
Alikhanyan Brothers 2, Yerevan 0036, Armenia*

E-mail: chili@aragats.am

ABSTRACT: We present the facilities of the Aragats Space Environmental Center in Armenia used during multi-year observations of the thunderstorm ground enhancements (TGEs) and corresponding environmental parameters. We analyze the characteristics of the detectors, operated on Aragats, and describe the coordinated detection of TGEs by the network of scintillators, field meters, and weather stations. By using a fast synchronized data acquisition system, we reveal correlations of the multivariate data on time scales from nanoseconds to minutes, which allow us to gain insight into the TGE and lightning origin and their interrelations. Also, we demonstrate how different coincidences of multilayered detector operation can select various species of secondary cosmic rays.

KEYWORDS: Large detector systems for particle and astroparticle physics; Particle identification methods

ARXIV EPRINT: [2204.01835](https://arxiv.org/abs/2204.01835)

*Corresponding author.

Contents

1	Introduction	1
2	Fast synchronized data acquisition system (FSDAQ)	2
3	STAND1 particle detector network on Aragats station	4
4	Synchronized registration of particle fluxes and radio emission from the atmospheric discharges	6
5	Simulation of the STAND1 detector response function. Coincidences of detector layers	9
6	Conclusions	13

1 Introduction

The high-energy physics in the atmosphere (HEPA) underwent a profound transformation in the last decade by accomplishing the correlated measurements of particle fluxes, fast wideband electric field records, and a variety of meteorological parameters, including near-surface electric field and geomagnetic field. The synergy between Cosmic Ray and Atmospheric physics lead to the development of models of the origin of particle bursts registered on the earth's surface, of the vertical profile of the strong electric field in the lower atmosphere, muon stopping effect, interrelations of particle fluxes and lightning flashes, circulation of Radon progeny in the atmosphere, and others. The successes of the multivariate measurements of the last decade put the HEPA on the priority research fields in both the Cosmic Ray and the Atmospheric physics communities. The HEPA research intensified the development of new methods of testing models and theories on atmospheric electricity, particularly in conditions that are related to the most important processes that influence earth's environments. Multi-messenger atmospheric science requires, first of all, the development of synchronized networks of identical sensors that are registering the multivariate data and which are stored in databases with open and fast access. The visualization and online correlation analysis of the big data coming from hundreds of measuring channels become a necessary tool in scientific research.

High-energy primary cosmic rays accelerated in violent stellar explosions in our galaxy are filling the space in a more-or-less stable nuclear composition, energy spectra, and density. Reaching the earth's atmosphere and interacting with nitrogen and oxygen atoms they produce extensive air showers (EASs) of different species of secondary cosmic rays (CR). Fluxes of secondary cosmic rays were studied in the last century and their energy spectra are well known at different latitudes and longitudes and heights above the atmosphere. Thunderstorm ground enhancements (TGEs, [1, 2]) observed mostly at mountain altitudes by a variety of particle detectors are large

impulsive enhancements in the intensity of electrons and gamma rays lasting from tens of seconds to tens of minutes. TGEs can be rather intense on the sharp mountain peaks sometimes enhancing (CR) background hundreds of times [3]. If the atmospheric electric field exceeds the critical value, specific to each air density (height in the atmosphere), electrons runaway and produces relativistic runaway electron avalanches (RREAs, [4]). The possible configurations of the intracloud electric field that initiated the RREA process are discussed in [5], see figure 1. Comparison of measured TGEs and simulations with GEANT4 and CORSIKA codes [6, 7] allows outlining the extension and strength of the electric field necessary for starting a runaway process, however, the horizontal extension of the electric field remains still not well understood. Measurements with several dosimeters installed at nuclear power plants in a coastal area of the Japanese sea made it possible to follow the source of the gamma ray flux moving with an ambient wind flow [8]. Using the muon stopping effect [9], the size of the particle emitting region was estimated at Nor Amberd research station, located on the slopes of Mt. Aragats at 2000 m height [10]. Estimates from both studies locate the horizontal dimension of the particle emitting regions within 1 km. However, in the recent radar-based gamma glow (TGE) study along the coast of the Japanese sea. it was observed that all TGEs were accompanied by the several km long radar echo regions indicating large lower positively charged regions [11]. Thus, the previously considered values of particle emitting region size seem to be highly underestimated. In the present paper, we describe the STAND1 particle detector’s network, operated on the Aragats research station aimed to estimate the size of the particle emitting region using a large collection of TGEs registered on Aragats. We are monitoring the secondary cosmic ray fluxes in a 24/7 regime and to avoid ionization losses within the station buildings, the STAND1 network is located outdoors under a 0.7 mm steel cover. This allows to establish a low energy threshold of the upper scintillator (≈ 1 MeV) but poses very stringent conditions on the reliability of detector operation under severe weather conditions.

2 Fast synchronized data acquisition system (FSDAQ)

Most Aragats particle detectors use plastic scintillators with a light-collecting diffuser in the form of a truncated pyramid [12]. At the top of the pyramid, there is a photomultiplier (PMT) with a large photocathode; at the base, there is usually a 5 cm thick scintillator. The big advantage of such a detector is a good amplitude resolution providing a dynamic range of $\approx 10^4$ for the measurements of flux intensity of extensive air shower (EAS) particles hitting the scintillator of a 1 m² area. The disadvantages include large vertical dimension and mass, and inhomogeneity of light collection at the edges of the scintillator.

Another design of light-collecting scintillator is based on spectrum-shifting fibers glued into the scintillator [13]. Photons of the scintillation flash, are re-emitted to the green part of the spectrum. The attenuation length of light in fiber optic fibers is up to 5 m, thus, the use of this technology allows for the design of the low-cost compact and light particle detectors.

For the STAND1 network, we use 1-m² sensitive area molded plastic scintillators fabricated by the High Energy Physics Institute, Serpukhov, Russia.

During thunderstorms changing particle count rates are correlated with the near-surface electrostatic field (NSEF). The Aragats area is continuously monitored by a network of commercially available electric field sensors (Model EFM-100, Boltek Corporation), three of which are placed at

the Aragats station, one at the Nor Amberd station at a distance of ≈ 13 km from Aragats, and one at the Yerevan station, at a distance of ≈ 39 km from Aragats. Three electric field mills at Aragats are located in the vertexes of a triangle with sides of 80 m, 270 m, and 290 m. The EFM-100 sensors are sensitive at distances not larger than 33 km, and the response time of the instrument is 100 ms. The electrostatic field changes are recorded at a sampling interval of 1s and 50 ms. For complete electrical isolation, the field mill is connected to the PC using a fiber optic cable.

The fast synchronized data acquisition (FSDAQ) provides detection of particle fluxes, the near-surface electric field disturbances, and waveforms of radio signals from atmospheric discharges, all harmonized with an accuracy of tens of nanoseconds. In figure 1 we show two systems of FSDAQ, (see details in [14]) operated in 2 experimental halls MAKET and SKL. Both systems employ a 2-channel digital storage oscilloscope (Picoscope 5244B) and National Instrument's NI-myRIO-1900 board. The NI-myRIO board that combines the Xilinx Zynq All Programmable SoC with a ready-to-go Linux-based real-time OS (RTOS), is used for synchronization of the data from particle detectors and wideband waveforms registered by electric mills and antennas.

The system in the SKL hall (figure 1a) includes synchronized measurements of electromagnetic emission produced by atmospheric discharges (fast wideband electric field) and the signal from a particle detector (NaI crystal or 3-cm thick plastic scintillator). The signal from the particle detector is fed to Ch A of the oscilloscope. The fast wideband electric field is registered by a circular flat antenna followed by a passive integrator the output of which is fed to Ch B of the same oscilloscope. The fast wideband electric field measurement system has a bandwidth of ≈ 50 Hz to 12.5 MHz (RC decay time constant 3 ms). The record length is 1 s, including a pre-trigger time of 200 ms and a post-trigger time of 800 ms. The sampling rate is 25 MS/s (40 ns sampling interval); the amplitude resolution is 8 bits. Starting from 2014, the fast wideband electric field data and particle data are stored on the ASEC servers and are available upon request. FSDAQ located in the SKL hall is triggered by a commercial MFJ-1022 active whip antenna that covers a frequency range from 300 kHz to 200 MHz.

The second FSDAQ system (figure 1b) located in MAKET experimental hall, is triggered by the abrupt enhancement of the particle flux (particle burst). The signal of the particle detector is fed to the NI MyRio board and, in parallel, to the oscilloscope. When the running mean of particle flux suddenly exceeds the preset background value by 20% (a TGE occurred), the NI MyRio board generates a master pulse for triggering the oscilloscope. The signals from the high-energy muon detector with an energy threshold of 250 MeV and a proportional counter of the Aragats neutron monitor are connected to A and B inputs of Picoscope. For both systems described above, the trigger-out pulse of the oscilloscope is relayed to the MyRIO board which produced the GPS timestamp of the record. A third MyRio board (without a digital oscilloscope, with a component form coinciding with the right part of FSDAQ) operates in the GAMMA experimental hall, where the third module of STAND1 detectors is installed.

MyRio boards located in the three experimental halls continuously register the 50-ns time series of the count rates registered by STAND1 modules. Additionally, at any triggering signal, each of the three MyRio boards generates an output signal containing the 50 ms count rates registered by 4 scintillators, near-surface electric field value, and, a GPS timestamp of the trigger signal. Thus, the fast waveform patterns are synchronized with particle fluxes and with slow (20 Hz) NSEF measurements.

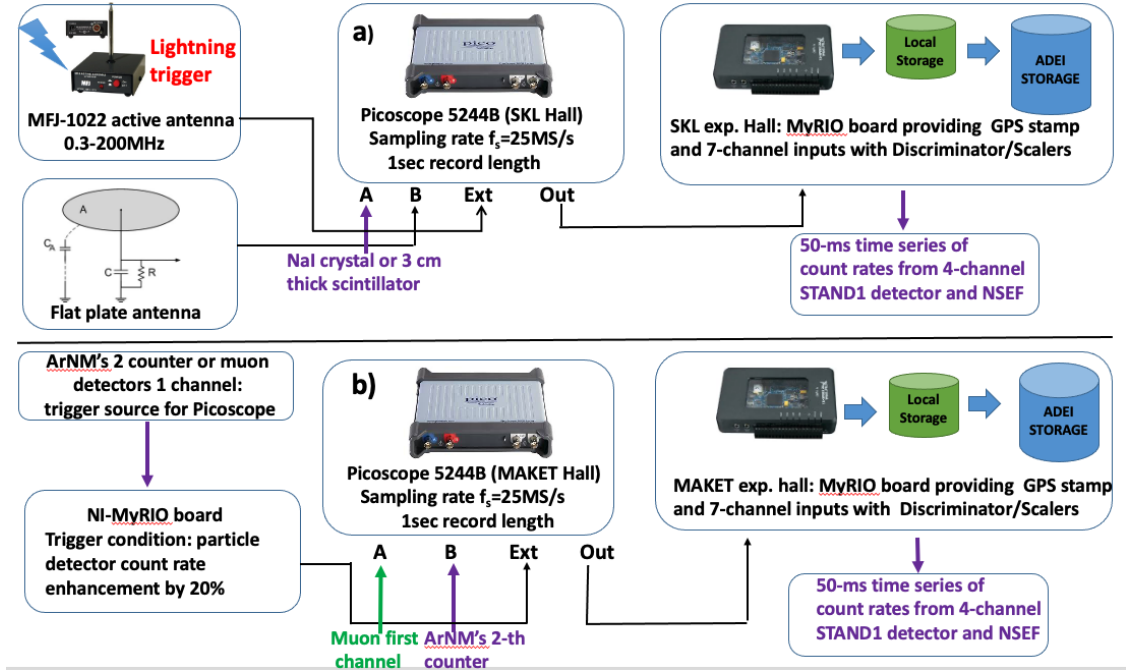


Figure 1. a) Component form of the fast synchronized data acquisition (FSDAQ) for the research of particle-lightning relations triggered by an atmospheric discharge (MAKET hall). b) The analogical system operating in SKL experimental hall and triggered by TGE.

For the location of lightning discharges in Aragats, we use a short-baseline Very High Frequency (VHF) interferometer system [15]. The interferometer (frequency range from 24 to 78 MHz) employs three identical circular flat-plate antennas of 30 cm diameter, which are located in the horizontal plane and form two orthogonal baselines of 13 m in length each. The cross-correlation functions are used to measure the azimuth and elevation angles of the radiation source as a function of time. The interferometer data are digitized at a 156.25 MS/s sampling rate (sample interval of 6.4 ns).

Data on the continuous monitoring of the particle fluxes and environmental parameters are available via advanced data extraction infrastructure (ADEI, <http://adei.crd.yerphi.am>).

3 STAND1 particle detector network on Aragats station

In figure 2a we show the location of the STAND1 network on Aragats station. All three identical units are located nearby three main experimental halls — MAKET, SKL, and GAMMA.

The “STAND1” detector is comprised of three layers of 1-cm-thick, 1-m² sensitive area scintillators stacked vertically and one 3-cm thick plastic scintillator of the same type stands apart; see figures 2b and 2c. The light from the scintillator through optical spectrum-shifter fibers is passed to the photomultiplier FEU-115M. The maximum luminescence is emitted at the 420-nm wavelength, with a luminescence time of about 2.3 ns. The STAND1 detector is tuned by changing the high voltage applied to the PMT and setting the thresholds for the discriminator shaper. The discrimination level is chosen to guarantee both high efficiency of signal detection and maximal suppression of photomultiplier noise.

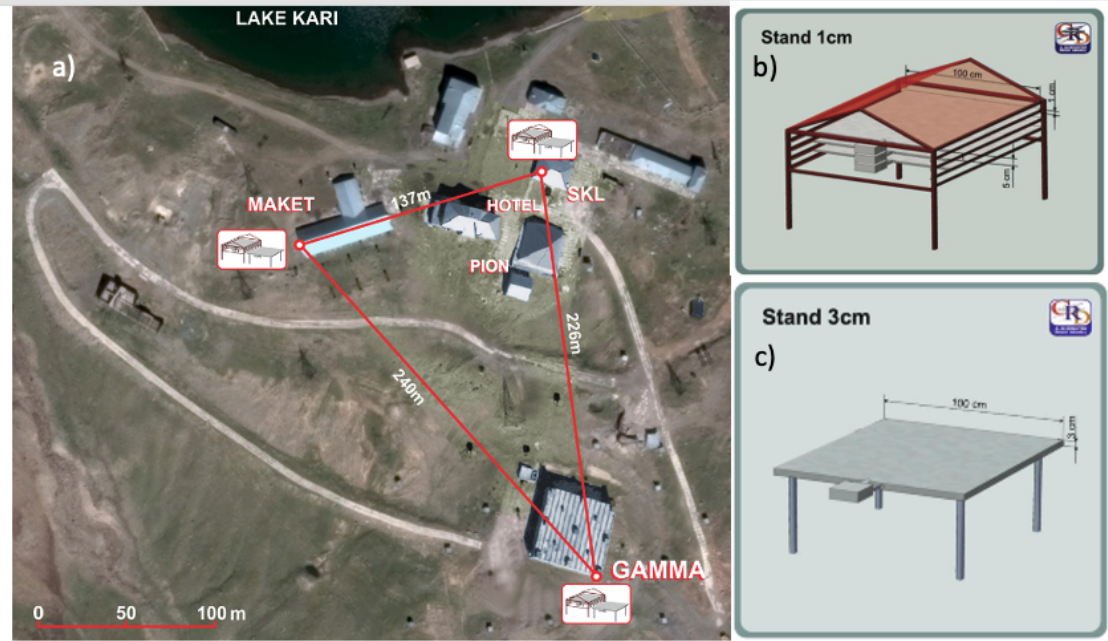


Figure 2. a) The map of Aragats station with STAND1 network; b) Stand1 unit: vertically stacked 1 cm thick, and 1 m^2 area plastic scintillators; c) Stand1 unit: stand-alone 3 cm thick plastic scintillator with the same area.

In figure 3 we show the typical shape of the pulse from the 1-cm thick scintillator of the STAND1 detector. As expected, the pulse is quite short, the full width on half maximum (FWHM) is less than 30 ns, and the maximum amplitude is reached in a few nanoseconds. This makes the detector very suitable for correlation studies with fast phenomena like lightning flashes.

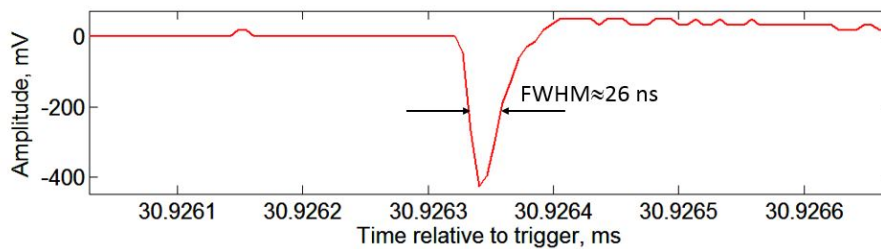


Figure 3. Typical time versus amplitude shape of the pulse from single particle registered by the 1-cm thick scintillator.

In figure 4 we show the response of the 1-cm thick scintillator to 10-MeV gamma rays and electrons obtained by GEANT4 simulations.

As we can see in figure 4 the efficiency of electron registration is much larger than the efficiency of gamma ray registration. By integrating the energy release spectra, we obtain $\approx 95\%$ for the electron registration efficiency and $\approx 3\%$ for the gamma ray. The modes of distribution are peaked at $\approx 2 \text{ MeV}$ (for electrons) and at $\approx 1.76 \text{ MeV}$ (for gamma rays). Thus, the 1-cm thick scintillators are perfectly suited for the measurement of the number of avalanche electrons in the detector.

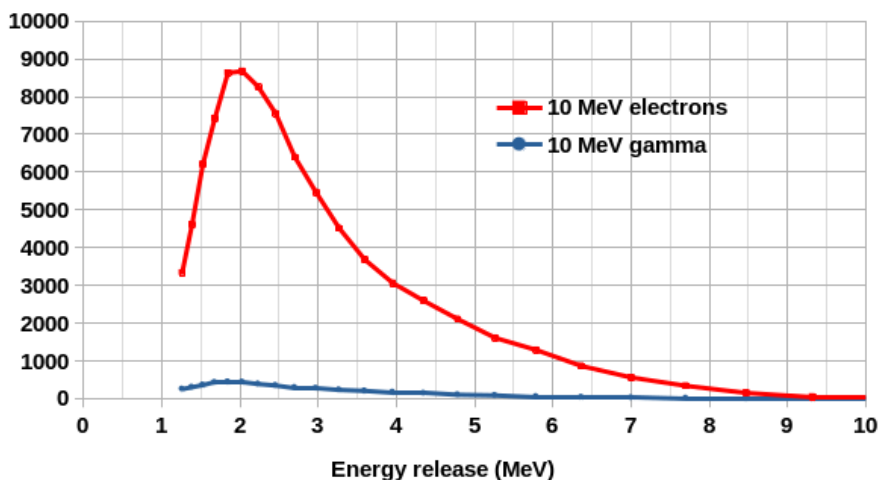


Figure 4. The response function (Y-axis — number of events fallen in each energy bin) of the 1-cm thick scintillator of STAND1 detector to 10-MeV electrons and gamma rays (100,000 simulation trials).

4 Synchronized registration of particle fluxes and radio emission from the atmospheric discharges

Synchronization of the STAND1 modules in different experimental halls by the FSDAQ electronics was checked with correlation analysis between all 3 remote modules (see figure 5 a, b, c). The operation of the STAND1 network was rather stable during Spring 2018. The mean values of 50-ms count rates from May 2 to June 2 were 23.7 ± 1.65 (GAMMA) and 24 ± 0.9 (MAKET), and 20 ± 3 (SKL); i.e., the relative errors were 7%, 2.7%, and 15%, respectively, which is rather satisfactory for such a short sampling.

In figure 5d we show 1-s time series of the upper scintillators of the STAND1 network from 18:28 to 18:34 during a thunderstorm that occurred on June 2nd. We can see a more-or-less smooth enhancement of the count rate by 67% ($\approx 10\sigma$) above the fair-weather value: the count rate increases from 460 to 767 counts per second (for the unit located on the roof of the GAMMA experimental hall, black curve). A large TGE was terminated by a lightning flash on a maximum phase of its development at 18:33.22:275 UT [16]. Count rate time series demonstrate coherent enhancement and termination, and in the scatter plots in the upper panel of figure 6(a–c) we see strong correlations of count rates measured by three independent scintillators (all correlation coefficients are larger than 0.85). Thus, the electron accelerator above the research station was operating uniformly in the atmosphere during 5 minutes of TGE, sending a large flux of electrons and gamma rays in the direction of the earth’s surface.

However, 1-s time synchronization shown in figure 5 is not enough for the joint analysis of particle fluxes and lightning occurrences usually terminated the particle flux (see collection of 165 TGEs abruptly terminated by a flash in the Mendeley data set [17]). In figure 6 and table 1 we show further analysis of TGE, now on a 50-ms time scale, registered during a total of 10 s. We can see that the abrupt termination of the TGE that exactly coincides for three STAND1 units on the 1-s time scale in figure 5, remains precisely coinciding also on the 50-ms time scale.

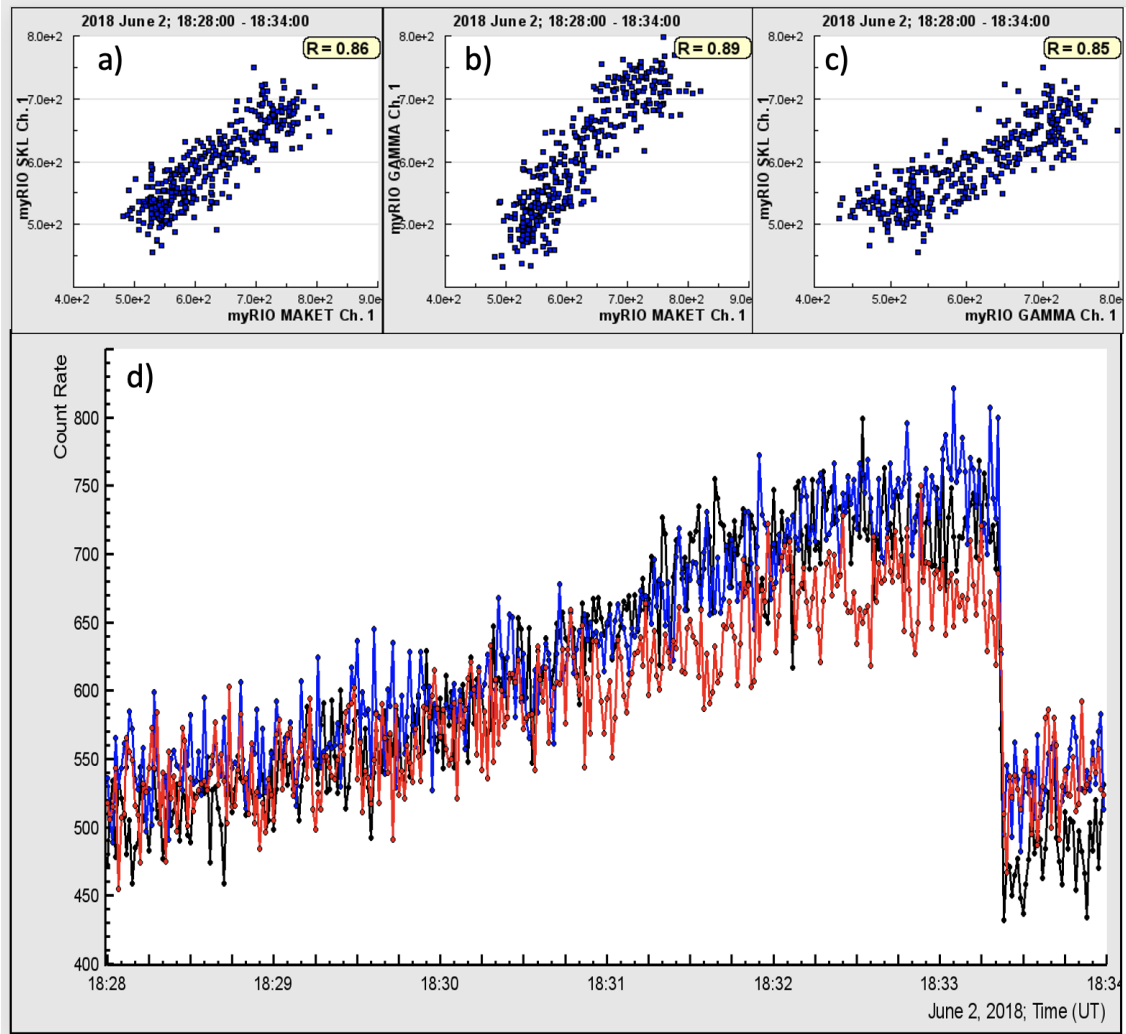


Figure 5. 1-s time series registered by the STAND1 network: GAMMA (black), MAKET (blue), SKL (red), for the module locations and distances see figure 2a. In the upper panel we show scatter plots of 1s count rates of STAND1 modules: a) scatter plot of MAKET-SKL; b) — the same for MAKET-GAMMA; c) the same for GAMMA-SKL; d) — 1-s time series of the upper scintillators of the STAND1 network.

However, the shapes and amplitudes of the disturbances of the NSEF are different, as well as the count rates of the 3 scintillators, see table 1.

In the second and third columns of table 1, we show the mean values of 50-s count rates before and after lightning flash, in the fourth column the surge of particle count rate, in the fifth and sixth — the NSEF measurements before the lightning flash, and at its local maximum. In the last column — the duration of the NSF surge from start to local maximum.

The differences in the local measurements of the NSEF are expected due to different locations on the mountain terrain. As was mentioned in [18] and in the references therein, the mountain geometry can strengthen the electric field by a factor on the order of 2. The location of NSEF sensors differs by the different height of the masts on which they are attached to, and the mountain environments also are different in different locations. Evidently, the scintillators are also not fully identical, and

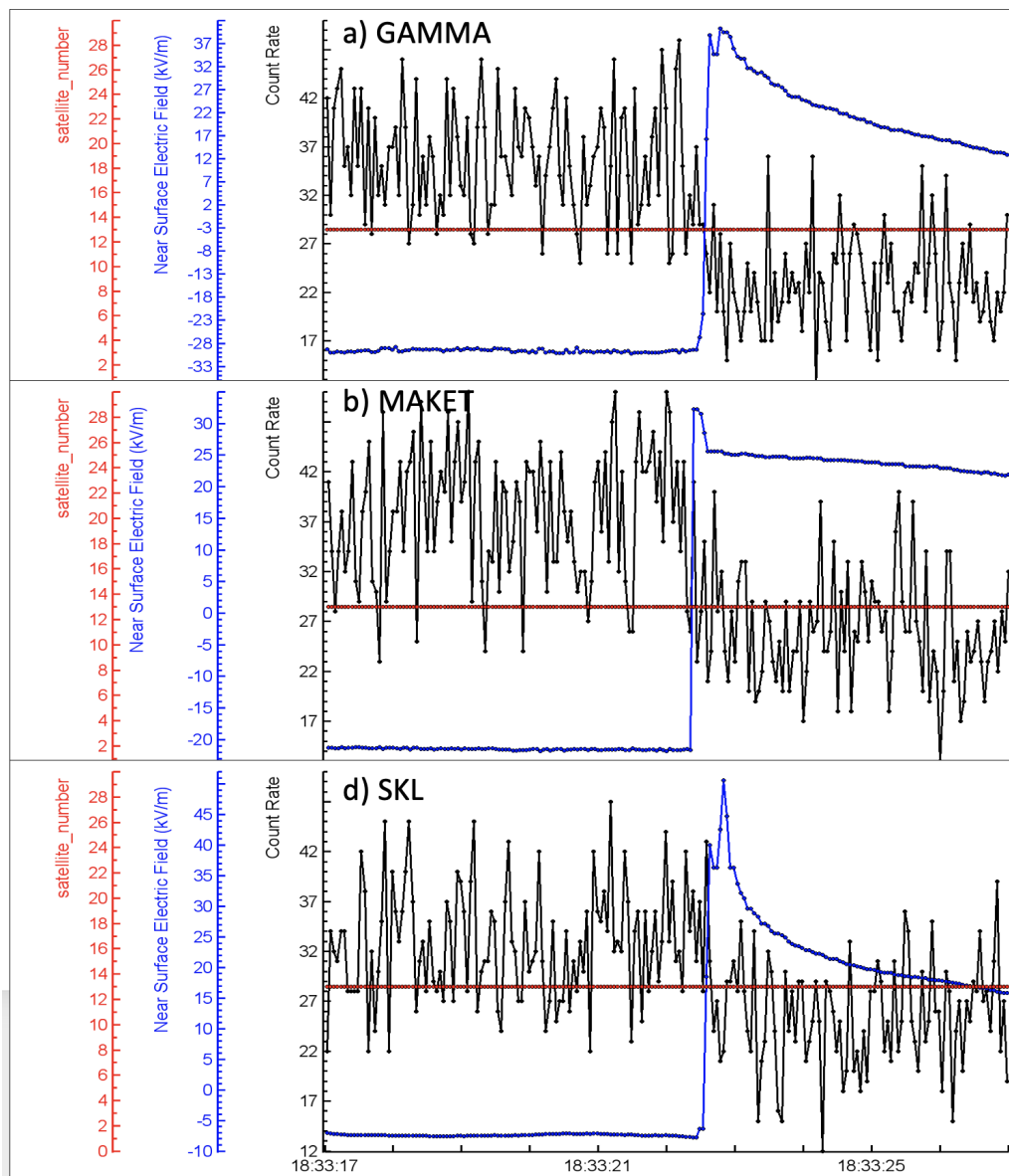


Figure 6. 50-ms time series of STAND1 network scintillators (black), disturbances of the NSEF, registered by the EFM-100 sensors (blue), and number of satellites used for the determination of GPS time stamps (red, 13 satellites operational for all STAND1 modules).

the high-voltages and discrimination thresholds can be altered during multi-year operation. Also, we are not dealing with man-made accelerators, with fixed bunches of particles. The atmospheric electron accelerator sends to the earth multiple RREA avalanches, that differ in acceleration lengths, electron, and gamma ray numbers, and maximum energies. A huge number of such avalanches constitute the enhanced particle fluxes that reach the earth's surface, and these enhanced fluxes can be stable on a second or even on a minute time scale. More detailed consideration of the particle fluxes and the disturbances of NSEF reveals complicated shapes and inhomogeneities of the NSEF measured by the network of EFM-100 electric mills [19].

Table 1. Parameters of particle fluxes and disturbances of NSEF registered during 10 s of maximum flux and termination of TGE, shown in figure 6.

18:33:17- 18:33:27	Mean before flash	Mean after flash	Surge of count rate	NSEF before flash (kV/m)	NESF after flash (kV/m)	NSEF surge	Duration of surge (ms)
GAMMA	29±8	20±11	9 (44%)	-29	38	67	200
MAKET	38±7	26±6	12(32%)	-21	32	53	50
SKL	33±6	25±5	8 (24%)	-7	50	57	100

Further zooming of synchronized detection of the pulses from particle detectors and atmospheric discharges is possible with high-speed oscilloscopes, using GPS timestamps produced by the NI MyRIO (FSDAQ system). We conduct experiments for years on Aragats to find particle bursts generated during the lightning flash. Despite a few observations reported in [20–24], we didn’t register any particle bursts coinciding with lightning flashes. Furthermore, numerous lightning flashes, registered on Aragats, do not originate TGEs but terminate them [16]. Our observations, well as a number of largest cosmic ray experiments, relate registered short particle bursts to well-known physical phenomena, namely extensive air showers [25–28]. To resolve this contradiction, and detect the possible generation of high-energy particles (with tens of MeV energies) in the lightning bolt, we measure simultaneously signals from a variety of particle detectors (NaI crystals, proportional chambers of neutron monitor, plastic scintillators) simultaneously with electromagnetic radiation from the atmospheric discharges (see details in [29, 30]). After multiyear observations, the only coincidences we detect were electromagnetic interferences (EMI). A lightning flash generates tens of kA currents in the atmosphere and, therefore, powerful electromagnetic radiation. If a flash happens nearby, it is rather difficult to screen any particle detector from this huge source of noise. Thus, some particle detectors generate pulses that can mimic the particle signals. However, if we look at the patterns of both EMI registered by antennas and particle output signals, we easily distinguish EMI from genuine particle bursts. In figure 7 we show a 70- μ s fragment of the synchronized registration of one of the NaI detector’s signals and the signals of the flat plate antenna by the same oscilloscope. The accuracy of synchronization is 40 ns (sampling interval of digitized signals).

We can see that NaI pulses (upper panel) ideally correlate with the fast electric field pulses (lower panel) and are bi-polar, whereas the genuine pulses from the particles registered by the large NaI crystal are unipolar and negative, as may be seen in figure 8. Thus, the “particle burst” registered by NaI, in fact, is an EMI signal induced in the detector circuit.

5 Simulation of the STAND1 detector response function. Coincidences of detector layers

The STAND1 detector located nearby the MAKET experimental is connected (in parallel to the NI MyRIO board) also to alternative electronics which makes it possible to register not only the count rates of detector layers but various combinations of their possible coincidences as well. In this way, we select different species of the ambient cosmic ray flux for further analysis. In table 2 we show the

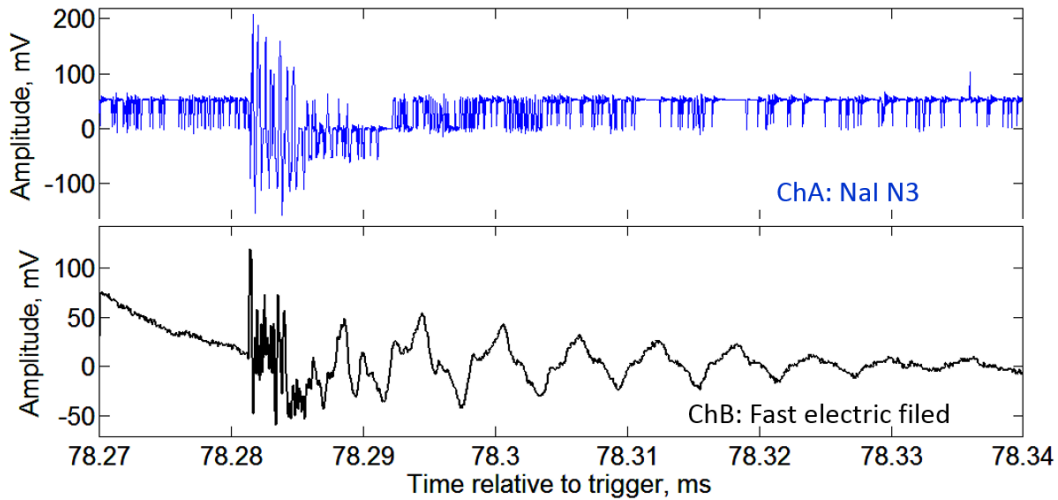


Figure 7. 40-ns time series of NaI spectrometer from the network operated in the SKL experimental hall (blue, channel A of picoscope), and the signals from the flat-plate antenna registering the electromagnetic radiation from atmospheric discharges (black, channel B of picoscope).

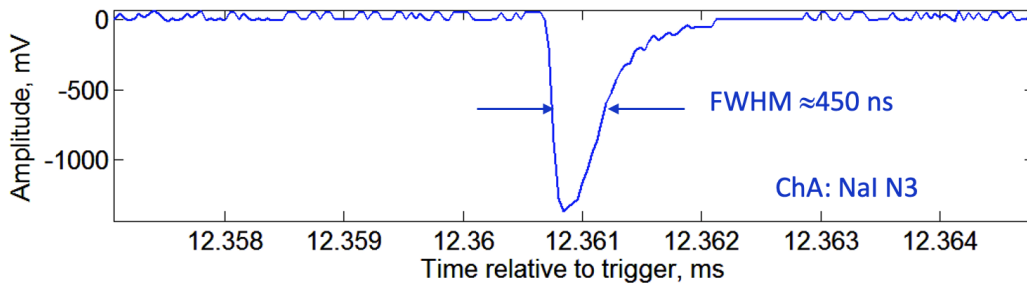


Figure 8. Typical shape of the signal generated by a particle in the large NaI crystal ($12 \times 12 \times 24$ cm).

results of detector response calculation with fluxes obtained from the EXPACS WEB calculator [31]. As we can see in table 2 the “001” coincidence (signal only in the bottom scintillator) and “010” coincidence (signal only in the middle scintillator) is enriched by neutral particles (neutrons and gamma rays), and the “111” coincidence (signals in all layers) selects charged particles (electrons, positrons, positive and negative muons). In the last column of table 2, we post the one-minute count rate of every coincidence. The 1-minute count rates of STAND1 layers, without any condition, are much larger 31600, 29500, and 27600.

Using the ADEI data analysis platform [32] we can readily obtain both online and archived data in graphical and numerical forms. In table 3 we post the background and TGE peak minute values of several STAND1 coincidences from our collection of TGE events. We choose the coincidences related to the lower layer for the analysis of the highest energies of TGE particles. First of all, we check that the sum of the coincidences, conditioned on the registration in the lower layer (namely 101, 011, 111, and 001) equals the overall count registered by the STAND1 lower layer. Then, we can examine the coincidences by comparing them with the data from table 2. For instance, we can see that 001 coincidence selects $\approx 95\%$ of the TGE gamma rays and only 5% electrons and

Table 2. The share of each of the species of cosmic ray background flux “selected” by different coincidences of the STAND1 scintillators.

Coincidence	Neutron %	Proton %	mu+ %	mu- %	Electron %	Positron %	Gamma %	1-minute count rate
001	20.46	0.56	4.02	3.57	1.90	1.96	67.53	4429
111	0.43	7.07	36.00	31.65	11.12	9.91	3.90	20149
110	3.10	4.77	17.51	15.16	25.59	17.49	15.94	3877
100	17.10	4.20	5.85	5.43	23.65	1376	30.01	7418
011	5.66	1.27	16.31	14.65	5.54	5.46	51.10	2581
101	4.10	1.12	36.56	31.70	12.77	11.06	2.70	1245
010	31.24	0.17	0.99	0.96	2.59	1.85	62.17	3431

positrons (other species of cosmic rays will not enhance during TGE). Thus, the enhancement of “001” coincidence can be related to the TGE gamma rays. In figure 9 (obtained from [33]) we can see that the energies of gamma rays selected by the “001” coincidence are larger than 10 MeV. Thus, we get an estimate of large energy gamma ray content in the TGE.

Table 3. The maximum and background values of the minute count rates of STAND1 coincidences for the TGE occurred at 18:33 on June 2, 2018.

Count rate	STAND1 Lower	STAND1 101	STAND1 011	STAND1 111	STAND1 001
TGE +background	20500	286	2469	12572	5173
Background	17199	233	2116	10797	4053
TGE	3301	53	353	1785	1170

Comparing STAND1 coincidences with registration efficiencies and shares of each species we can estimate the content of particle species in the TGE. If the TGE is large, as we can see in figure 10 (“100” coincidence’s enhancement reaches 55%), we recover energy spectra of charged and neutral components of TGE with the Aragats solar neutron telescope (ASNT, [34]). ASNT is a 60 cm thick and 4 m² area spectrometer measuring separately electron and gamma ray differential energy spectra using a “veto” option with the upper 5 cm thick scintillator of the same area. Due to ionization losses in the air, the electron flux attenuates very fast and the majority of TGE particles are gamma rays. Only if a very strong (≈ 2 kV/cm) electric field extends 1000–2000 m the highest energy electrons can reach particle detectors located on 3200 m a.s.l. Therefore, for the majority of TGEs, the gamma ray flux highly surpasses the electron flux. However, using coincidences in the STAND1 layers, we can reliably select as well TGEs with sizable electron content. Comparing data of STAND1 coincidences and electron energy spectra obtained from ASNT we confirm very rare and very informative “electron” TGEs. After recovering energy spectra, we can obtain by simulation count rates of all STAND1 coincidences and double-check obtained electron energy spectrum.

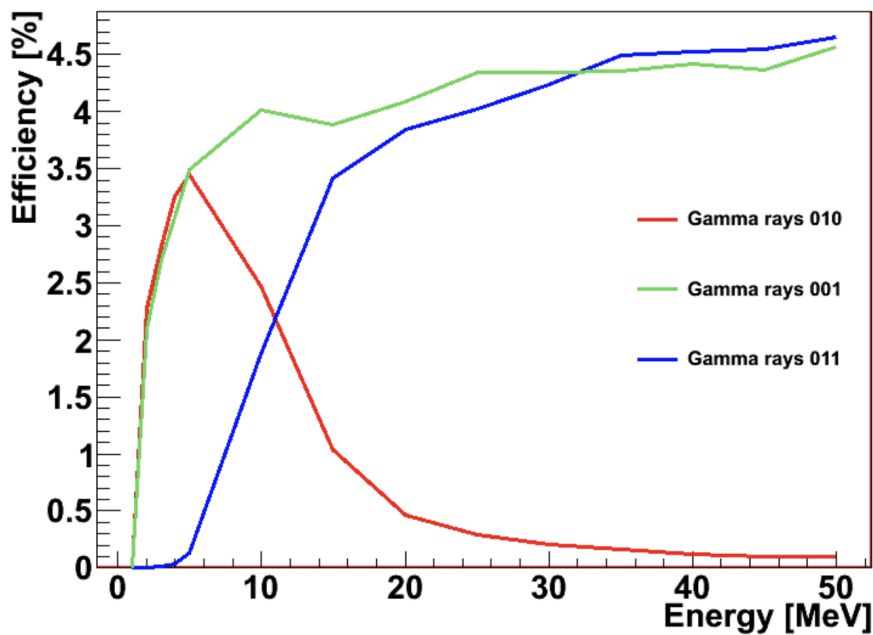


Figure 9. The energy dependence of different STAND1 coincidences to register gamma rays.

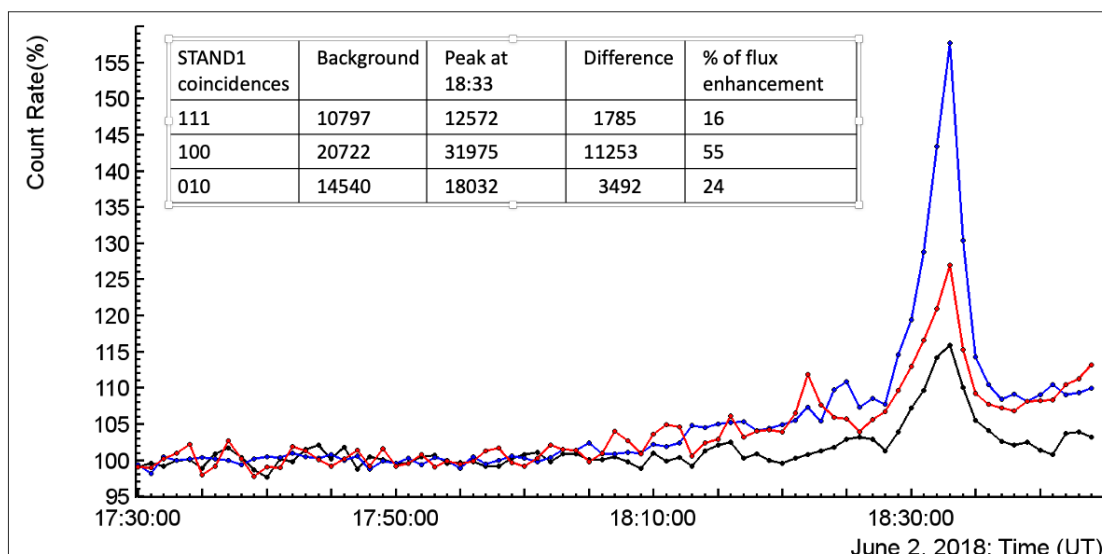


Figure 10. 1-minute time series of count rates of STAND1 coincidences.

In figure 11 we demonstrate another possibility of the analysis of the STAND1 detector's coincidences. By dividing counts of 101 coincidence by 111 coincidence counts at fair weather and during TGE we estimate the efficiency of the middle scintillator to be 97–98%.

In figure 12, we show one more possibility of STAND1 data analysis. As we see from the figure, the enhancement of the gamma ray flux (selected by 001 coincidence) started at 17:45 long before the TGE maximum at 18:33. The disturbances of the NSEF just started and cannot initiate TGE, however, the ^{226}Rn progeny, which are attached to charged aerosols are lifted by the NSEF and cause enhancement of the count rate of the lower STAND1 detector's scintillator [35].

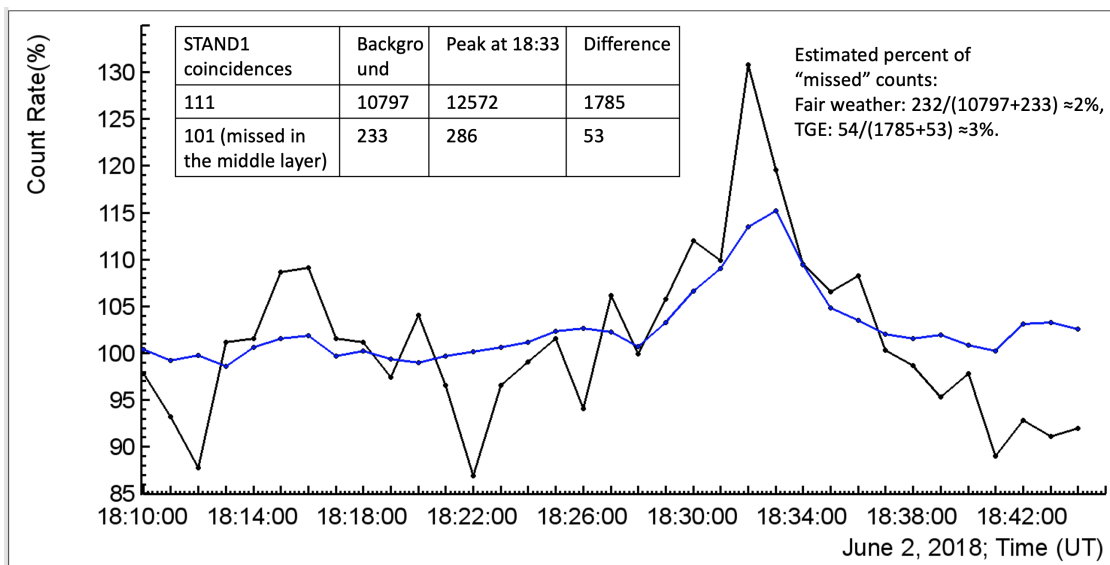


Figure 11. Comparison of efficiency of the middle scintillator of STAND1 at fair weather and during TGE. Black curve — 101 coincidence, blue curve 111 coincidence.

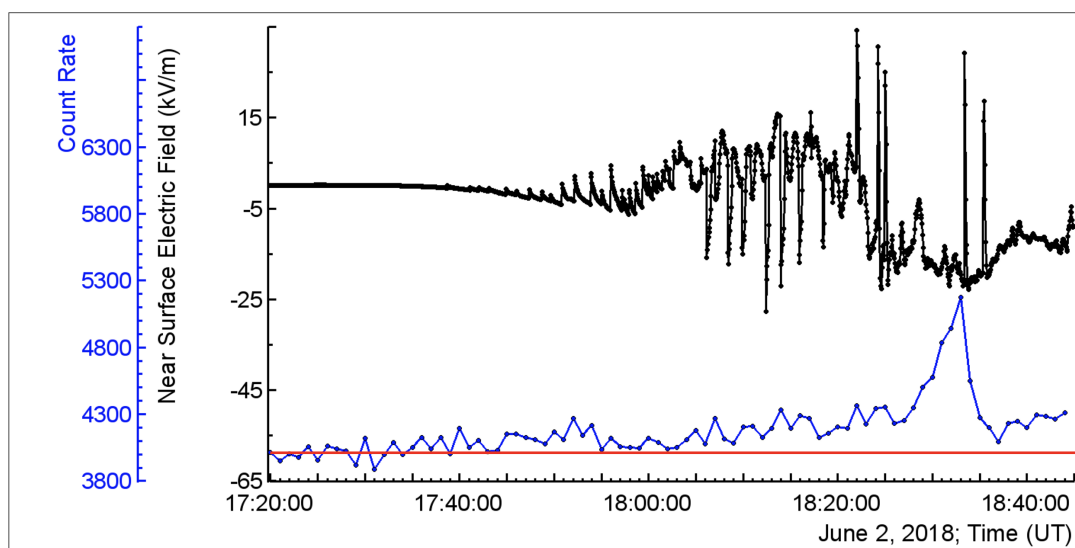


Figure 12. Time series of disturbances of NSEF (black curve) and count rate of 001 STAND1 coincidence. By the red line we show that the enhancement of count rate started at 17:45 long before the TGE start.

6 Conclusions

The progress in the High Energy Physics in the Atmosphere (HEPA) research has been pushed by establishing the networks of the same type of particle detectors at different sites at Aragats Space Environmental Center and in the countries of Eastern Europe and Germany. The joint operation of these networks has shown that TGEs is a universal process sharing the same characteristics measured at different observation sites, and can be explained by the conventional electron runaway

phenomenon [4]. Target-like experiments with particle detectors located on the earth’s surface allow TGE registration in all detail, including energy spectra of electrons, and gamma rays, their spatial distribution, and relation to the lightning flashes and environmental parameters. EAS physics and HEPA are synergistically connected and need to exchange results for the explanation of particle bursts and for revealing the influence of atmospheric electric fields on the EAS shape and size.

The comparisons of the delayed correlations between the signals from the network of scintillation detectors and local disturbances of the near-surface electric field measured by electric field mills open the possibility of mapping the vertical and horizontal profiles of the atmospheric electric field. The correlations of STAND1 modules during large TGE on June 2nd (figure 5) demonstrate that at least over an area of $\approx 10^6$ m² fluxes of TGE particles are identical and, therefore vertical atmospheric electric field can sustain for minutes strengths of 2.0–2.2 kV/cm, providing TGE particle fluxes up to 300 particles per second, and for the extreme values of the atmospheric electric field — up to 30,000 particles per second [3].

Analysis of the 1 s and 1-minute time series of STAND1 coincidences allows us to identify the TGE event, and estimate its significance, spatial extension, and TGE electron content.

Multiyear monitoring of the lightning flashes and particle fluxes on 50 ms and nanosecond time scales with FSDAQ electronics (figure 1) allows rejecting the hypothesis of the “lightning origin” of TGE (figure 7, [25]). Lightning flashes abruptly stop TGE (figure 6), not originate MeV particles.

On milliseconds time scales we can observe inhomogeneities of the NSEF reflecting the approaching storm and peculiarities of mountain terrain.

Registered coincidences of STAND1 layers give additional possibilities to separate different species of the cosmic ray flux, for researching the muon stopping effect, neutron production during thunderstorms, and others . “111” coincidence selects charged particles with $\approx 90\%$ purity; “010” coincidence selects neutral particles with $\approx 95\%$ purity; “001” coincidence selects high-energy gamma rays with $\approx 70\%$ purity (see table 2).

Acknowledgments

We thank the staff of the Aragats Space Environmental Center for the uninterrupted operation of experimental facilities on Aragats under severe weather conditions. The data for this study is available in numerical and graphical formats by the multivariate visualization software platform ADEI on the WEB page of the Cosmic Ray Division (CRD) of the Yerevan Physics Institute, <http://adei.crd.yerphi.am/adei> and from Mendeley datasets [14, 26]. The authors acknowledge the support of the Science Committee of the Republic of Armenia (research project No 21AG-1C012), in the modernization of the technical infrastructure of high-altitude stations.

Declaration of competing interest. The authors declare no conflict of interest.

Data availability statement. The data for this study are available in numerical and graphical formats on the WEB page of the Cosmic Ray Division (CRD) of the Yerevan Physics Institute, <http://adei.crd.yerphi.am/adei> and from Mendeley datasets [17, 30].

References

- [1] A. Chilingarian et al., *Ground-based observations of thunderstorm-correlated fluxes of high-energy electrons, gamma rays, and neutrons*, *Phys. Rev. D* **82** (2010) 043009.
- [2] A. Chilingarian, G. Hovsepyan and A. Hovhannisyanyan, *Particle bursts from thunderclouds: Natural particle accelerators above our heads*, *Phys. Rev. D* **83** (2011) 062001.
- [3] R. Chum et al., *Significant enhancements of secondary cosmic rays and electric field at high mountain peak during thunderstorms*, *Earth Planets Space* **72** (2020) 28.
- [4] A.V. Gurevich, G.M. Milikh and R. Roussel-Dupre, *Runaway electron mechanism of air breakdown and preconditioning during a thunderstorm*, *Phys. Lett. A* **165** (1992) 463.
- [5] A. Chilingarian, G. Hovsepyan and M. Zazyan, *Measurement of TGE particle energy spectra: An insight in the cloud charge structure*, *Europhys. Lett.* **134** (2021) 69001.
- [6] GEANT4 collaboration, *GEANT4 — a simulation toolkit*, *Nucl. Instrum. Meth. A* **506** (2003) 250.
- [7] S. Buitink, T. Huege, H. Falcke, D. Heck and J. Kuijpers, *Monte Carlo simulations of air showers in atmospheric electric fields*, *Astropart. Phys.* **33** (2010) 1 [arXiv:0910.5268].
- [8] T. Torii, T. Sugita, M. Kamogawa, Y. Watanabe and K. Kusunoki, *Migrating source of energetic radiation generated by thunderstorm activity*, *Geophys. Res. Lett.* **38** (2011) 1.
- [9] A. Chilingarian, G. Hovsepyan, G. Karapetyan and M. Zazyan, *Stopping muon effect and estimation of intracloud electric field*, *Astropart. Phys.* **124** (2021) 102505.
- [10] A. Chilingarian, N. Bostanjyan and T. Karapetyan, *On the possibility of location of radiation-emitting region in thundercloud*, *J. Phys. Conf. Ser.* **409** (2013) 012217.
- [11] Y. Wada et al., *Meteorological aspects of gamma-ray glows in winter thunderstorms*, *Geophys. Res. Lett.* **48** (2021) e2020GL091910.
- [12] A. Chilingarian, G. Gharagozyan, G. Hovsepyan, S. Ghazaryan, L. Melkumyan and A. Vardanyan, *Light and heavy cosmic-ray mass group energy spectra as measured by the MAKET-ANI detector*, *Astrophys. J.* **603** (2004) L29.
- [13] G.I. Britvich et al., *The large scintillation charged particles detector of the Tien-Shan complex 'ATHLET'*, *Nucl. Instrum. Meth. A* **564** (2006) 225.
- [14] D. Pokhsroryan, *Fast Data Acquisition system based on NI-myRIO board with GPS time stamping capabilities for atmospheric electricity research*, in *Proceedings of TEPA symposium*, Nor-Amberd, Armenia (2015), pg. 23.
- [15] A. Chilingarian, M. Dolgonosov, A. Kiselyov, Y. Khanikyants and S. Soghomonyan, *Lightning observations using broadband VHF interferometer and electric field measurements*, *2020 JINST* **15** P07002.
- [16] A. Chilingarian, Y. Khanikyants, V.A. Rakov and S. Soghomonyan, *Termination of thunderstorm-related bursts of energetic radiation and particles by inverted-polarity intracloud and hybrid lightning discharge*, *Atmosph. Res.* **233** (2020) 104713.
- [17] S. Soghomonyan, A. Chilingarian and Y. Khanikyants, *Dataset for Thunderstorm Ground Enhancements terminated by lightning discharges*, *Mendeley Data* **V1** (2021).
- [18] W.W. Hager and W. Feng, *Charge rearrangement deduced from nearby electric field measurements of an intracloud flash with K-changes*, *J. Geophys. Res. Atmos.* **118** (2013) 10,313.

- [19] A. Chilingarian, G. Hovsepyan, T. Karapetyan, B. Sargsyan and E. Svechnikova, *Transient Luminous Events in the lower part of the Atmosphere originated in the Peripheral Regions of a Thunderstorm*, [arXiv:2205.02822](https://arxiv.org/abs/2205.02822).
- [20] S. Mallick, V.A. Rakov and J.R. Dwyer, *A study of X-ray emissions from thunderstorms with emphasis on subsequent strokes in natural lightning*, *J. Geophys. Res. Atmos.* **117** (2012) D16107.
- [21] M.D. Tran et al., *A terrestrial gamma-ray flash recorded at the Lightning Observatory in Gainesville, Florida*, *JASTP* **136** (2015) 86.
- [22] J.R. Dwyer et al., *A ground level gamma-ray burst observed in association with rocket-triggered lightning*, *Geophys. Res. Lett.* **31** (2005) L05119.
- [23] J.W. Belz et al., *Observations of the Origin of Downward Terrestrial Gamma-Ray Flashes*, *J. Geophys. Res. Atmos.* **125** (2020) e2019JD031940.
- [24] Y. Wada et al., *Characteristics of low-frequency pulses associated with downward terrestrial gamma-ray flashes*, *Geophys. Res. Lett.* **49** (2020) e2021GL097348.
- [25] HAWC collaboration, *On the sensitivity of the HAWC observatory to gamma-ray bursts*, *Astropart. Phys.* **35** (2012) 641 [[arXiv:1108.6034](https://arxiv.org/abs/1108.6034)].
- [26] Z.T. Izhbulyakova et al., *Investigation of the EAS neutron component with the URAN array: first simulation and experimental results*, *J. Phys. Conf. Ser.* **1690** (2020) 012071.
- [27] A.P. Chubenko et al., *New complex EAS installation of the Tien Shan mountain cosmic ray station*, *Nucl. Instrum. Meth. A* **832** (2016) 158 [[arXiv:1912.13356](https://arxiv.org/abs/1912.13356)].
- [28] ARGO-YBJ and PRISMA collaborations, *Detection of thermal neutrons with the PRISMA-YBJ array in Extensive Air Showers selected by the ARGO-YBJ experiment*, *Astropart. Phys.* **81** (2016) 49 [[arXiv:1512.01326](https://arxiv.org/abs/1512.01326)].
- [29] A. Chilingarian, S. Soghomonyan, Y. Khanikyanc and D. Pokhsraryana, *On the origin of particle fluxes from thunderclouds*, *Astropart. Phys.* **105** (2019) 54.
- [30] S. Soghomonyan, A. Chilingarian and D. Pokhsraryana, *Extensive Air Shower (EAS) registration by the measurements of the multiplicity of neutron monitor signal*, *Mendeley Data* **V1** (2021).
- [31] T. Sato, *Analytical model for estimating the zenith angle dependence of terrestrial cosmic ray fluxes*, *PLOS ONE* **11** (2016) e0160390.
- [32] S. Chilingaryan, A. Chilingarian, V. Danielyan and W. Eppler, *The Aragats data acquisition system for highly distributed particle detecting networks*, *J. Phys. Conf. Ser.* **119** (2008) 082001.
- [33] B. Mailyan, *The efficiencies of the Aragats space environmental center (ASEC) particle detectors used in thunderstorm ground enhancement (TGE) research*, ADEI WiKi, <http://adei.crd.yerphi.am/setups/asec/pictures/Efficiencies.pdf>.
- [34] A. Chilingarian, G. Hovsepyan, T. Karapetyan, B. Sargsyan and S. Chilingaryan, *Measurements of energy spectra of relativistic electrons and gamma-rays from avalanches developed in the thunderous atmosphere with Aragats Solar Neutron Telescope*, *2022 JINST* **17** P03002 [[arXiv:2201.10134](https://arxiv.org/abs/2201.10134)].
- [35] A. Chilingarian, G. Hovsepyan and B. Sargsyan, *Circulation of Radon progeny in the terrestrial atmosphere during thunderstorms*, *Geophys. Res. Lett.* **47** (2020) e2020GL091155.